Nighttime nitric oxide densities in the Southern Hemisphere mesosphere–lower thermosphere

P. E. Sheese,[1] R. L. Gattinger,[2] E. J. Llewellyn,[2] C. D. Boone,[3] and K. Strong[1]

[1]   Observations of NO_2 continuum nightglow emissions from OSIRIS, on board the Odin satellite, have been used to derive an eight-year time series of Southern Hemispheric nitric oxide densities, [NO]. OSIRIS is one of the very few current satellite instruments deriving ground state [NO] during the polar winter. The production of NO in this region is strongly dependent on energetic particle precipitation (EPP), and densities are therefore observed to vary with solar activity. Between 2003 and 2009, mean Antarctic winter [NO] in the mesosphere–lower thermosphere decreased by a factor of 3.7, and now, after the prolonged solar minimum that spanned 2008–2009, [NO] in this region is on the rise. As solar activity increases in the next few years, the production of NO is expected to increase. As downward advection readily transports NO_x into the lower mesosphere and stratosphere, such an increase will lead to a greater potential for stratospheric ozone loss. **Citation:** Sheese, P. E., R. L. Gattinger, E. J. Llewellyn, C. D. Boone, and K. Strong (2011), Nighttime nitric oxide densities in the Southern Hemisphere mesosphere–lower thermosphere, *Geophys. Res. Lett.*, *38*, L15812, doi:10.1029/2011GL048054.

1. Introduction

[2]   Nitric oxide (NO) is an important trace species in the Earth's upper atmosphere, as it plays a significant role in determining the structure of the lower ionosphere and strongly influences the overall energy budget of the lower thermosphere. As well, NO_x ($NO + NO_2$) in the mesosphere–lower thermosphere (MLT) is transported downwards into the stratosphere, where it destroys ozone catalytically. The deposition of MLT polar winter NO_x into the stratosphere has been a topic of great interest over the past three decades [e.g., *Solomon et al.*, 1982; *Russell et al.*, 1984; *Siskind et al.*, 2000]. It is estimated that in the Arctic and Antarctic winter, NO_x deposited into the stratosphere from the MLT makes up 5–9% [*Funke et al.*, 2005; *Reddmann et al.*, 2010] of that region's total reactive nitrogen (NO_y) budget. Model results of *Reddmann et al.* [2010] demonstrated that these NO_x intrusions can lead to significant and persistent stratospheric ozone loss. *Randall et al.* [2009] showed that even during periods of low levels of energetic particle precipitation (EPP), the meteorological conditions of the middle atmosphere can still lead to increased deposition of MLT NO_x into the stratosphere.

[3]   The Optical Spectrograph and Infrared Imaging System (OSIRIS) is a limb-viewing instrument on board the Odin satellite that was launched into orbit in early 2001. The optical spectrograph observes scattered sunlight and airglow emissions over a spectral range of 275–810 nm with ~1 nm spectral resolution, and scans the Earth's limb between tangent heights of 7–110 km with a vertical resolution of 1 km and a pointing accuracy of ~0.5 km. The NO_2 continuum, produced by the chemiluminescent reaction $NO + O (+ M) \rightarrow NO_2 (+ M) + h\nu$, is detected by OSIRIS in the winter MLT at tangent heights above 85 km and solar zenith angles greater than 102°. *Gattinger et al.* [2009] used OSIRIS observations of the NO_2 continuum over the wavelength range of 400–800 nm to derive continuum volume emission rate (VER) profiles, and *Gattinger et al.* [2010] also derived continuum VER profiles from OSIRIS observations in order to retrieve [NO] profiles for a sample period of 8–9 May 2005. This study extends the OSIRIS retrievals, forming a time series of Southern Hemispheric [NO] that spans the autumn and winter months of 2003–2010, and reports on the initial analysis of the dataset.

2. Methodology

[4]   The NO_2 VER retrieval technique is described in detail by *Gattinger et al.* [2009, 2010]. In brief, model OH Meinel band and atomic oxygen green line spectra are removed from the OSIRIS observations of the NO_2 continuum between 430–710 nm. The remaining spectrum is fit to a reference model spectrum [*Becker et al.*, 1972] to determine the limb brightness at 580 nm, the spectral peak. The limb brightness profile at 580 nm is multiplied by the 450 nm equivalent spectral width of the continuum [*Becker et al.*, 1972] and inverted to determine the total continuum (370–1400 nm) VER profile. Derivations of [NO] from the continuum VER require the reaction coefficient of the bimolecular reaction $NO + O \rightarrow NO_2 + h\nu$ ($k_1 = 4.2 \times 10^{-18}$ cm^3 molecule^{-1} s^{-1} [*Becker et al.*, 1972]), the reaction coefficient of the termolecular reaction $NO + O + M \rightarrow NO_2 + M + h\nu$ ($k_2 = 15.5 \times 10^{-33}$ exp(1160/1.987T) cm^6 molecule^{-2} s^{-1} [*Whytock et al.*, 1976]), and background densities, [M], obtained from a locally run MSIS-E-00 model [*Picone et al.*, 2002]. Retrievals also require accurate atomic oxygen density, [O], and temperature profiles, which are derived from simultaneous common volume OSIRIS measurements of the O_2 A-band at 762 nm [*Sheese et al.*, 2010, 2011]. *Gattinger et al.* [2010] determined the root-sum-square systematic error of the [NO] retrievals to be on the order of 30%; sources of systematic error included error in the reaction coefficients, MSIS background densities and temperatures, and the OSIRIS A-band [O]

[1]Department of Physics, University of Toronto, Toronto, Ontario, Canada.
[2]ISAS, Department of Physics and Engineering Physics, University of Saskatchewan, Saskatoon, Saskatchewan, Canada.
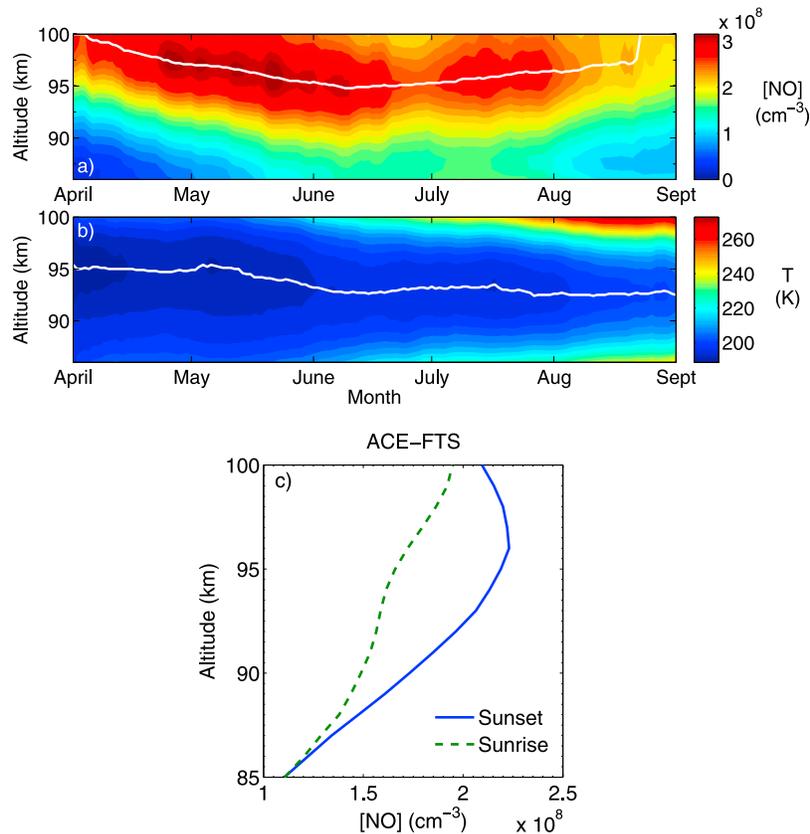[3]Department of Chemistry, University of Waterloo, Waterloo, Ontario, Canada.

Figure 1. Antarctic 2003–2010 composite time series of (a) retrieved [NO] profiles (white line indicates height of peak [NO]) and (b) simultaneously derived A-band temperature profiles (white line indicates height of mesopause). Both datasets have been smoothed with a 30-day triangular filter. (c) April-August 2004–2010 mean ACE-FTS [NO] profiles for sunset (blue) and sunrise (green) conditions in the Antarctic.

retrieval. The difference between retrieved [NO] values using A-band temperatures and those from MSIS is typically on the order of ±10%.

[5] At heights above 100 km and below 85 km, the OSIRIS signal-to-noise ratio in the A-band nightglow emission measurements is not large enough for reliable retrievals of [O] and temperature values. Therefore, [NO] retrievals are limited to the altitude range of 85–100 km. Only Southern Hemisphere data is presented in this paper as the OSIRIS mission has only recently started observing the Northern Hemisphere nighttime in the MLT region.

3. Results

[6] Figures 1 and 2 show the nighttime [NO] climatology in the Southern Hemisphere. The climatologies were determined using all OSIRIS 2003–2010 observations, both AM and PM. However between 2003 and 2006 OSIRIS only sampled the MLT approximately one day out of ten, whereas between 2007 and 2010 the MLT was sampled every other day. Therefore, the climatologies are biased towards the later years of the mission.

[7] Figure 1 shows derived time series of [NO] and A-band temperature profiles at high latitudes (60–90°S) from April to August. Data in both time series have been smoothed with a 30-day triangular filter in order to highlight the 5-month variation. [NO] peak heights (mesopause heights) were determined by taking the maximum (minimum) values of profiles

spline interpolated to 0.1 km intervals. At the beginning of April, [NO] peaks above the maximum OSIRIS NO retrieval altitude of 100 km, which is consistent with the accepted peak near 106 km [*Bailey et al.*, 2002]. The peak height, indicated by the white line in Figure 1a, steadily decreases to an altitude of 95 km in mid-June. During the winter months, the peak height increases back to above 100 km in late August. The mesopause height, indicated by the white line in Figure 1b, shows a similar trend, descending from 95 km to 93 km in the autumn months, and the MLT warms throughout the winter due to adiabatic
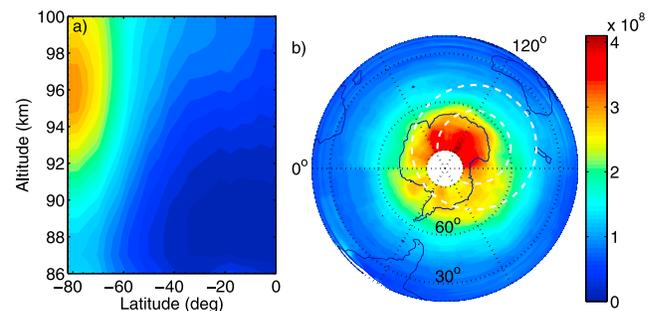

Figure 2. 2003–2010 [NO] composites. (a) Latitudinal cross section of zonally averaged [NO] profiles. (b) Southern Hemispherical map of [NO] at an altitude of 96 km, dashed white lines indicate the inner and outer edges of the Southern auroral oval.
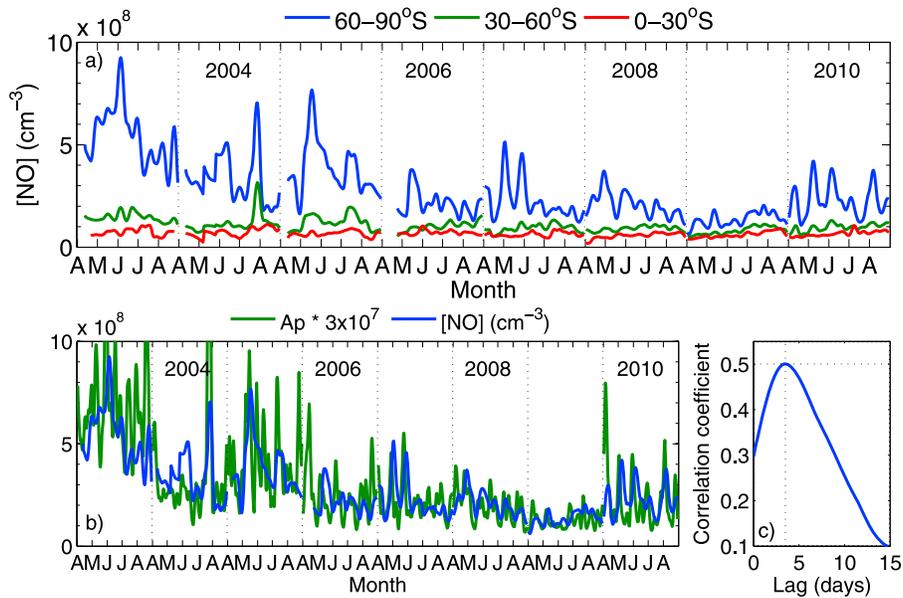
Figure 3. (a) Vertical mean (90–100 km) time series of [NO] at high, mid, and low latitudes in the Southern Hemisphere. Data are smoothed with a 10-day triangular filter. (b) Time series of Southern Hemispheric high-latitude [NO] and scaled A_p index values, both smoothed with 10-day triangular filter. (c) Correlation between the high-latitude [NO] time series and the time-shifted A_p index time series.

heating associated with downward motion. During the same time period, [NO] is observed to decrease at all altitudes and appears to be in an inverse relationship with temperature. However, correlation coefficients between daily average temperatures and [NO] were calculated at each altitude level and showed that there is no anti-correlation between temperature and [NO] at any altitude between 85–100 km.

[8] Mean peak heights of [NO] in the non-polar regions (Figure 2) are above 100 km, which is consistent with measurements from other missions. The low polar [NO] peak height, near 95 km, has not previously been observed nor predicted by model simulations. However, Atmospheric Chemistry Experiment – Fourier Transform Spectrometer (ACE-FTS) [*Bernath et al.* 2005] version 2.2 NO data [*Boone et al.*, 2005; *Kerzenmacher et al.*, 2008] does exhibit a similar feature. The 2004–2010 April-August Antarctic mean profiles for both sunset and sunrise conditions are shown in Figure 1c, however it should be noted that due to the orbital geometry ACE has no Antarctic data from mid-June to mid-July. The profiles show that at sunrise conditions the [NO] peak is typically above 100 km, however at sunset conditions the [NO] peak is typically near 96 km, which is consistent with the nighttime OSIRIS observations. Further investigation is needed into why modelled polar night [NO] profiles do not exhibit such a low peak height.

[9] A latitudinal cross section of zonally averaged profiles is shown in Figure 2a. As expected, [NO] is greatest in the polar region where NO production is strongly dependent on EPP, and decreases with latitude towards the equator where NO production is driven by the solar soft X-ray irradiance. Figure 2b shows the zonal variation at an altitude of 96 km. In the polar region there is a clear [NO] dependence on longitude, with densities peaking near 80°S, 119°E. This region is above the South geomagnetic pole (80°S, 108°E) and is confined to the same approximate geo-location as the Southern auroral oval. Increased production of NO near the

South geomagnetic pole is a phenomenon observed each year at heights above 90 km.

[10] As NO production in the MLT is dependent on solar activity, it is expected that [NO] will vary with the 11-year solar cycle. Figure 3a shows the time series of the 90-100 km mean [NO] in the high, mid, and low Southern latitudes (60–90°S, 30–60°S, and 0–30°S, respectively); data have been smoothed with a 10-day triangular filter in order to limit noise effects and produce continuous curves in the 2003–2006 data. The variation in the time series is most evident at high latitudes where 5-month mean values are seen to decrease by a factor of 3.7 from 2003 (seasonal mean [NO] = 5.23 × 10^8 cm^{-3}) to 2009 (seasonal mean [NO] = 1.41 × 10^8 cm^{-3}). In the mid and low latitudes, 5-month mean values decreased by a factor of 1.8 and 1.4 respectively over the same time period.

[11] As NO production in the polar region is dominated by auroral particles, the retrieved [NO] dataset has been compared to a time series of A_p index values, a proxy for geomagnetic activity. Daily A_p index values were obtained from the National Geophysical Data Center website (http://www.ngdc.noaa.gov). The A_p data, scaled and smoothed with a 10-day triangular filter, is shown in Figure 3b along with the 90–100 km high-latitude time series of Figure 3a. The datasets are moderately correlated, both with a periodicity of roughly 25 days. However, since only high-energy particles precipitate below 100 km, the majority of NO is produced at higher altitudes and transported down into the MLT. The lag time between [NO] and A_p suggests that the downward transport time is on the order of 0–2 weeks. Using 2007–2010 three-day averages of A_p and vertical mean [NO], correlation coefficient values were calculated by comparing the two datasets, with the A_p data time shifted by a range of lag times. The largest correlation between the two datasets, $r = 0.5$, was calculated with an A_p lag time of 3.5 days, as seen in Figure 3c. This same procedure was
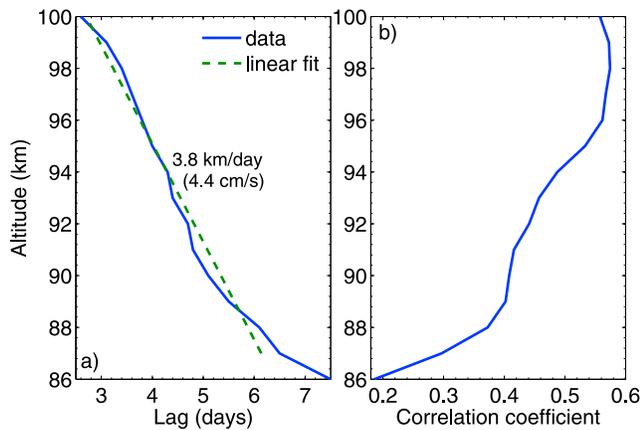
Figure 4. Results of correlation coefficient calculations, comparing three-day average A_p index and [NO] values as a function of altitude. (a) Vertical profile of time shifts in A_p data that yielded the largest correlation coefficients. (b) Vertical profile of maximum correlation coefficients.

performed using the same three-day average A_p data but correlated with three-day average [NO] values at each altitude from 86–100 km. It can be seen in Figure 4 that the lag time in A_p that yields the peak correlation coefficient decreases approximately linearly with decreasing altitude, from 2.6 days at 100 km to 7.5 days at 87 km. The lag time profile serves as a proxy for the mean seasonal EPP generated NO (EPP-NO) descent rate in the MLT. A linear fit to the lag profile between 87–100 km yields a descent rate of 3.8 km/day (4.4 cm/s).

4. Summary and Discussion

[12] OSIRIS is one of the few satellite instruments to have a current database of nighttime winter [NO] in the Southern Hemisphere MLT. Both the Sub-Millimetre Radiometer (SMR) on board Odin and the Michelson Interferometer for Passive Atmospheric Sounding (MIPAS) on Envisat retrieve daytime and nighttime NO concentrations in the MLT, however open literature results of polar winter [NO] are not yet available. The retrieved OSIRIS database spans April to August of 2003–2010, over an altitude range of 85–100 km. In the climatology, the peak height of [NO] descends to altitude of 95 km near winter solstice, which is a much lower peak height than has been previously measured (outside the polar winter region) by other satellite missions. Both the peak height of [NO] and the mesopause height are observed to descend on the order of a few kilometers between April and June. There is, however, no correlation between [NO] and temperature measurements, and both phenomena are attributable to the mean downward motion that is typical of this region—hence the consistent warming observed in the climatology. Since the mean meridional flow is directed poleward, the decrease in [NO] after winter solstice seen in the climatology (apart from a slight increase in mid-July) is most likely due to increasing hours of sunlight leading to increased photodissociation/photoionization of NO in the region. Due to increased EPP, the zonal mean values are greatest in the high latitudes and decrease with decreasing (equatorward) latitude at all altitudes. Similarly, in the high latitudes at altitudes above 90 km, the longitu-

dinal variation is such that there is an increase in [NO] near the auroral oval, roughly above the geomagnetic pole. This is a clear indication of what has been known now for decades, that NO in this region is produced predominantly via auroral particles, where the majority of EPP-NO observed at the lower altitudes, below ~95 km, was most likely produced at higher altitudes.

[13] Production of nighttime NO in the MLT is dependent on solar activity, and densities significantly decreased from 2003 to 2009 in response to decreasing solar activity. As solar activity is now increasing, OSIRIS is already observing increases in nighttime MLT region [NO]. *Randall et al.* [2009] demonstrated that stratospheric ozone loss due to the injection of MLT region NO_x can occur even during periods of low solar activity, given the right dynamical conditions in the middle atmosphere. Therefore, an increase of polar nighttime [NO] in the MLT may not lead to further stratospheric ozone loss, however, the potential for increased ozone loss will be greater in the next few years of the solar cycle.

[14] A proxy EPP-NO descent rate in the Antarctic MLT was derived by correlating [NO] values to time shifted A_p index values. A descent rate of 3.8 km/day was determined, which is much larger than the upper stratosphere–lower mesosphere NO_x descent rate of a few hundred meters per day [*Funke et al.*, 2005; *Randall et al.*, 2007, 2009]. This is not unexpected, as average vertical wind speeds are typically much lower in this region than in the MLT. Vertical wind speeds in the winter MLT are typically presumed to be on the order of 2 cm/s, however both upward and downward vertical winds in high latitude MLT regions are known to reach much higher speeds, on the order of 10 m/s, on a daily basis [e.g., *Smith and Hernandez*, 1995; *Höffner and Lautenbach*, 2009; *Bhattacharya and Gerrard*, 2010]. Clearly the OSIRIS MLT NO descent rate is inconsistent with typical mean mesospheric wind speeds. A future study will investigate both daytime and nighttime NO concentrations from Odin and ACE observations, and will compare the measurements to model simulations in order to elucidate MLT NO descent rates.

References

Bailey, S. M., C. A. Barth, and S. C. Solomon (2002), A model of nitric oxide in the lower thermosphere, *J. Geophys. Res.*, *107*(A8), 1205, doi:10.1029/2001JA000258.
Becker, K. H., W. Groth, and D. Thran (1972), The mechanism of the air-afterglow NO + O → NO_2 + $h\nu$, *Chem. Phys. Lett.*, *15*, 215–220, doi:10.1016/0009-2614(72)80152-0.
Bernath, P. F., et al. (2005), Atmospheric Chemistry Experiment (ACE): Mission overview, *Geophys. Res. Lett.*, *32*, L15S01, doi:10.1029/2005GL022386.
Bhattacharya, Y., and A. J. Gerrard (2010), Wintertime mesopause region vertical winds from Resolute Bay, *J. Geophys. Res.*, *115*, D00N07, doi:10.1029/2010JD014113.

Boone, C. D., R. Nassar, K. A. Walker, Y. Rochon, S. D. McLeod, C. P. Rinsland, and P. F. Bernath (2005), Retrievals for the atmospheric chemistry experiment Fourier-transform spectrometer, *Appl. Opt.*, *44*, 7218–7231, doi:10.1364/AO.44.007218.

Funke, B., M. López-Puertas, S. Gil-López, T. von Clarmann, G. P. Stiller, H. Fischer, and S. Kellmann (2005), Downward transport of upper atmospheric NO_x into the polar stratosphere and lower mesosphere during the Antarctic 2003 and Arctic 2002/2003 winters, *J. Geophys. Res.*, *110*, D24308, doi:10.1029/2005JD006463.

Gattinger, R. L., W. F. J. Evans, I. C. McDade, D. A. Degenstein, and E. J. Llewellyn (2009), Observation of the chemiluminescent $NO + O \rightarrow NO_2 + h\nu$ reaction in the upper mesospheric dark polar regions by OSIRIS on Odin, *Can. J. Phys.*, *87*, 925–932, doi:10.1139/P09-051.

Gattinger, R. L., et al. (2010), NO_2 air afterglow and O and NO densities from Odin-OSIRIS night and ACE-FTS sunset observations in the Antarctic MLT region, *J. Geophys. Res.*, *115*, D12301, doi:10.1029/2009JD013205.

Höffner, J., and J. Lautenbach (2009), Daylight measurements of mesopause temperature and vertical wind with the mobile scanning iron lidar, *Opt. Lett.*, *34*, 1351–1353, doi:10.1364/OL.34.001351.

Kerzenmacher, T., et al. (2008), Validation of NO_2 and NO from the Atmospheric Chemistry Experiment (ACE), *Atmos. Chem. Phys.*, *8*, 5801–5841, doi:10.5194/acp-8-5801-2008.

Picone, J. M., A. E. Hedin, D. P. Drob, and A. C. Aikin (2002), NRL-MSISE-00 Empirical model of the atmosphere: Statistical comparisons and scientific issues, *J. Geophys. Res.*, *107*(A12), 1468, doi:10.1029/2002JA009430.

Randall, C. E., V. L. Harvey, C. S. Singleton, S. M. Bailey, P. F. Bernath, M. Codrescu, H. Nakajima, and J. M. Russell (2007), Energetic particle precipitation effects on the Southern Hemisphere stratosphere in 1992–2005, *J. Geophys. Res.*, *112*, D08308, doi:10.1029/2006JD007696.

Randall, C. E., V. L. Harvey, D. E. Siskind, J. France, P. F. Bernath, C. D. Boone, and K. A. Walker (2009), NO_x descent in the Arctic middle atmosphere in early 2009, *Geophys. Res. Lett.*, *36*, L18811, doi:10.1029/2009GL039706.

Reddmann, T., R. Ruhnke, S. Versick, and W. Kouker (2010), Modeling disturbed stratospheric chemistry during solar-induced NOx enhancements observed with MIPAS/ENVISAT, *J. Geophys. Res.*, *115*, D00I11, doi:10.1029/2009JD012569.

Russell, J., III, S. Solomon, L. Gordley, E. Remsberg, and L. Callis (1984), The variability of stratospheric and mesospheric NO_2 in the polar winter night observed by LIMS, *J. Geophys. Res.*, *89*, 7267–7275, doi:10.1029/JD089iD05p07267.

Sheese, P. E., E. J. Llewellyn, R. L. Gattinger, A. E. Bourassa, D. A. Degenstein, N. D. Lloyd, and I. C. McDade (2010), Temperatures in the upper mesosphere and lower thermosphere from OSIRIS observations of O_2 A-band emission spectra, *Can. J. Phys.*, *88*, 919–925, doi:10.1139/P10-093.

Sheese, P. E., I. C. McDade, R. L. Gattinger, and E. J. Llewellyn (2011), Atomic oxygen densities retrieved from Optical Spectrograph and Infrared Imaging System observations of O_2 A-band airglow emission in the mesosphere and lower thermosphere, *J. Geophys. Res.*, *116*, D01303, doi:10.1029/2010JD014640.

Siskind, D. E., G. E. Nedoluha, C. E. Randall, M. Fromm, and J. M. Russell III (2000), An assessment of Southern Hemisphere stratospheric NO_x enhancements due to transport from the upper atmosphere, *Geophys. Res. Lett.*, *27*, 329–332, doi:10.1029/1999GL010940.

Smith, R. W., and G. Hernandez (1995), Vertical winds in the thermosphere within the polar cap, *J. Atmos. Terr. Phys.*, *57*, 611–620, doi:10.1016/0021-9169(94)00101-S.

Solomon, S., P. J. Crutzen, and R. G. Roble (1982), Photochemical coupling between the thermosphere and the lower atmospherez: 1. Odd nitrogen from 50 to 120 km, *J. Geophys. Res.*, *87*, 7206–7220, doi:10.1029/JC087iC09p07206.

Whytock, D. A., J. V. Michael, and W. A. Payne (1976), Absolute rate constants for $O + NO + N_2 \rightarrow NO_2 + N_2$ from 217–500 K, *Chem. Phys. Lett.*, *42*, 466–471, doi:10.1016/0009-2614(76)80655-0.

C. D. Boone, Department of Chemistry, University of Waterloo, 200 University Ave. W., Waterloo, ON N2L 3G1, Canada.

R. L. Gattinger and E. J. Llewellyn, ISAS, Department of Physics and Engineering Physics, University of Saskatchewan, 116 Science Pl., Saskatoon, SK S7N 5E2, Canada.

P. E. Sheese and K. Strong, Department of Physics, University of Toronto, 60 St. George St., Toronto, ON M5S 1A7, Canada. (psheese@atmosp.physics.utoronto.ca)